Size and dopant dependent single particle fluorescence properties of carbon nanodots

Somes K. Das[a, †], Chi Man Luk[c], William E. Martin[a], Libin Tang[c], Doo Young Kim[a], Shu Ping Lau[c], and Christopher I. Richards[a]*

[a]Department of Chemistry, University of Kentucky, 505 Rose Street, Lexington KY 40506,

[c]Department of Applied Physics, The Hong Kong Polytechnic University, Hong Kong SAR.

*chris.richards@uky.edu

KEYWORDS: Graphene quantum dot, Carbon nanodot, fluorescence, single molecule imaging, graphene.

Abstract: The emissive properties of both doped and non-doped carbon nanodots (CNDs) with sizes ranging from 3-11 nm were analyzed at the single particle level. Both doped and non-doped CNDs are a composite of particles exhibiting green, red, or NIR fluorescence on excitation at 488, 561, and 640 nm, respectively. Nitrogen doped CNDs (N-CNDs) with diameters ranging

from 3.4 to 5.2 nm show a larger proportion of particles with NIR emission as compared to nondoped particles. Doping of CNDs also resulted in changes in the photostability and the fluorescence intermittency seen in single CND particles. While ms to sec time scale blinking was regularly observed for red emitting non-doped CNDs, nitrogen doping significantly reduced blinking. Both doped and non-doped particles also exhibit moderate size dependent photophysical properties.

Introduction

Carbon nanodots (CNDs) have attracted growing interest in recent years due to their low cost, processibility, chemical stability, and photostability[1-3]. Because of their tunable fluorescence and excellent biocompatibility, these particles have also been proposed as ideal fluorescent probes for bio-imaging[4-6]. CNDs exhibit wavelength dependent fluorescence where the emission spectra shifts as the excitation wavelength changes suggesting further utility[7]. Seeking to take advantage of these properties, many groups have generated CNDs of different size and with various dopants demonstrating fluorescence ranging from the UV to near-infrared (NIR) regions[8]. Interestingly, ensemble photophysical measurements show that CND properties depend on the synthetic method[9-15]. As a result the origin of the luminescence in these particles has been attributed to several mechanisms including excitons of carbon, emissive traps, quantum confinement effect, aromatic structures, oxygen containing groups, free zigzag sites and edge defects[16-22]. While the exact mechanism of the observed photo-luminescence is still not fully understood[23], steady state spectra have consistently shown that the emission of bulk samples change with the excitation wavelength[24]. Many reports attribute these optical properties to changes in energy levels that scale with the size of the CND[25,26] or doping of the CND[27]. Other studies propose that a single

CND particle contains multiple emissive states leading to the observation of excitation wavelength dependent emission in bulk samples[9,15,23]. A previous report of single particle fluorescence of carbon nanodots with diameters ranging from ~3 to 8 nm found that isolated single CNDs did not exhibit fluorescence at multiple wavelengths but did show multi-chromophoric behavior[7]. This suggested that separate particles might be responsible for the emission at different excitation wavelengths rather than a single particle emitting at multiple wavelengths[28]. As shown in ensemble photoluminescence data, the emission spectra of CNDs shift with the excitation wavelength, indicating that CNDs are broadly distributed in terms of HOMO-LUMO gap. Single particle measurements allow the photoselection of a fraction of CNDs with similar properties. Here we utilize ensemble and single molecule fluorescence techniques to compare the properties of non-doped and nitrogen doped CNDs with emission in the visible and near infrared regions.

Experimental Methods

Materials: Poly (vinyl alcohol), (PVA, Avg. Mol. Wt. 95000) and sodium hydroxide were both obtained from Thermo Fisher Scientific NJ, USA. Cover-slips used for microscopy were purchased from Gold Seal Products (Portsmouth, NH, USA). Absolute 200 proof ethanol used for cleaning the glass cover slips was from AAPER Alcohol and Chemical Co. (Shelbyville, KY, USA). PBS buffer was purchased from Amresco Inc., OH, USA and used after dilution. All buffers were filtered by using cellulose acetate filters (0.2 mm) from VWR Intl. (IL, USA). Glucose (≥99.5%) and ammonium hydroxide solution (25% NH_3) were purchased from Sigma-Aldrich without further purifying.

Preparation of CNDs and N CNDs: Both non-doped CNDs and N-CNDs were prepared by the

microwave-assisted hydrothermal method. For the preparation of non-doped CNDs, the glucose solution (3 *wt*%) was siphoned to a glass bottle with a tightened cover. The solution was irradiated in a microwave reactor (CEM Discover SP) at 300 W with a fixed time of 5 minutes at 180 °C. The size of the CNDs can be tuned in the range from 3 to 11 nm by adjusting the reaction pressure from 165 to 350 psi. The fabrication process of the N-CNDs was similar to that of the CNDs, except that aqueous ammonia (25%) was used as solvent. The N content in the N-CNDs was controlled by changing the concentration of the ammonia solution in the solvent. The reaction temperature and pressure were kept at 180 ℃ and 200 psi respectively. In addition, the size could be increased with increasing the reaction pressure, while keeping the ammonia concentration constant. The size of the CNDs was determined by a transmission electron microscopy (JEOL, JEM-2100F). The N/C ratio of the N-CNDs was obtained by electron energy loss spectroscopy.

Immobilization of CNDs on Glass: CNDs, both non-doped and nitrogen doped, were immobilized on a cleaned glass coverslip by spiking a ~ nano-molar concentration of the CNDs in poly vinyl alcohol (PVA) and spin coating on the coverslip. PVA solution (1 gram/ml) was prepared in PBS buffer at pH 7.5. Microscope cover-slips were cleaned by immersing in NaOH (5.0 M) for about 30 min. Before use cover-slips were washed thoroughly in ultrapure water, rinsed in ethanol and dried with filtered nitrogen gas.

Single-molecule microscopy: Laser light (561 nm, 640 nm or 488 nm) was directed into a 1.49 NA Olympus ApoN oil-immersion (Type F, ne 1.518) 60X objective (Olympus America, Center Valley, PA, USA) mounted on an Olympus IX 81- inverted microscope (Olympus America). The intensity of the 561 nm laser was adjusted to ~78 W cm^2. Fluorescence emission was collected through the microscope objective and separated from the incident laser by using Green Filter set:

laser cleaner: FF01-561-14, dichroic: Dio1-R488/561-25×36 emission: FF01-609/54-25 (Semrock, Rochester, NY, USA) or Red Filter set: Laser line cleaner: FF01-640-14, dichroic: Di02-R635-25x36, emission: BLP01-664R-25 or Blue filter set: 51022 - EGFP/mRFP-1 from Chroma Inc. Data were typically collected for ~3-7 min at 100 ms exposure time by using a cooled (-80ºC) ANDOR iXon3 CCD camera (Andor Technology, South Windsor, CT USA) and Metamorph (Molecular Devices, LLC., Sunnyvale, CA, USA) software. All data were recorded at room temperature (25ºC). The shapes of the fluorescence spots are irregular because of fluorescence intensity fluctuations of the individual molecules and the number of molecules differs from frame to frame because of dark states. To overcome this we recorded 5 frames and then averaged the intensities and subtracted the background. Single-molecule events from wide field images were extracted from the stream acquisition of 2000 frames at 100 ms exposure time. This was done by integrating the intensity of 3×3 pixel area around isolated fluorescent spots using Metamorph or ImageJ (NIH, USA) and then subtracting the background.

Analyses of single level, multiple fluorescence levels, and blinking: We used intensity distribution histograms of individual time traces to define multiple versus single fluorescence level particles. Gaussian distributions for individual time traces were analyzed in the same way as was reported before[7]. Single step bleaching molecules were characterized by 2 well defined Gaussian distributions- 1 corresponding to the background level and 1 corresponding to a single emission intensity level. Distribution histograms of particles showing multiple levels of fluorescence exhibited 3 or more distributions. Additionally, we examined each time trace by setting a level duration and intensity difference threshold to define separate fluorescence levels. A unique fluorescence level was defined as lasting for at least 1 sec and levels were defined as

separate levels if they were separated by 3 times the square root of the average counts (N) of a specific fluorescence level. Additionally, a fluorescence level was required to be separated from the background level by at least 3 times the square root of the average background counts. All events shorter than 1 sec or with a fluorescence amplitude separated by less than 3(√N) from the level transitioned from or to were defined as transient events not corresponding to a discrete fluorescence level. This analysis agreed with the assignment of single or multi-level fluorescence from distribution histograms.

Average intensity measurements: The intensities of single particles were measured over time during exposure with laser light an an epi configuration with EMCCD detection. The histogram of such intensities of each group of particles was fit to a Gaussian distribution and the peak of the Gaussian fit was taken as the average intensity of that set of particles. The errors are obtained from the Gaussian fits of the single particle intensities of each set of average sized particles (Figures 4S and 5S).

Photobleaching time measurements: The photobleaching time of single non doped CNDs or N-CNDs were measured from the decay curve obtained from their decrease in numbers in a field of view during laser light illumination. These data were collected on the immobilized CNDs on PVA film and exposed ~80 W/cm^2 power. Time traces of photobleaching were recorded at 100 ms exposure time by widefield imaging at the single particle level (Figures 6S and 7S).

Steady state emission and excitation spectra measurements: CNDs were dispersed in PBS buffer and pH was adjusted to 8.0. Emission and excitation spectra were measured by Fluoromax 4 (Horiba Scientific). Bandwidths of emission and excitation monochro-mators were set to 5 nm.

The emission and excitation spectra were corrected using a built in correction factor of the instrument (Figure 8S).

Results and Discussion

Recent reports have shown that the fluorescence properties of CNDs are changed when doped with nitrogen or sulfur[29-32]. One interesting feature of this work was the observation of CNDs giving fluorescence in the NIR. Using ensemble measurements other groups have also reported size dependent fluorescence properties of CNDs with diameters ranging from 5 nm to 35 nm[33]. To determine the effect of size on the photophysical properties of non-doped and N-CNDs (~3 nm to ~12 nm), we isolated particles in a thin film of PVA (polyvinyl alcohol) on a glass cover slip. TEM was used to determine CND size (Supporting information Figure 4S). We then imaged individual particles using 488 nm, 561 nm, and 640 nm excitation. At bulk concentrations, solution based measurements with 488 nm excitation showed high levels of fluorescence. However, when samples were diluted to single particle levels no signal was detected above the background level indicating the individual particles are not bright enough to be observed with 488 nm excitation. However, with both 561 nm and 640 nm excitation individual molecules were clearly visible. To determine if the same particles exhibited fluorescence at both 561 nm and 640 nm excitation we imaged identical fields of view with both wavelengths for all species of CNDs. Overlaying the images taken at 561 and 640 nm excitation showed no overlap between particles from these two channels (Figure 1). This indicated that no particle possessed chromophores which can be excited by both 561 nm and 640 nm within the same particle. This was consistent for non-doped (Figure 1 A, B, and C) as well as doped (Figure 1 D, E, and F) particles. This same observation was observed for all of samples we tested (Supporting Information, Figure 1S). We also compared the fluorescence intensities of individual non-doped and nitrogen doped

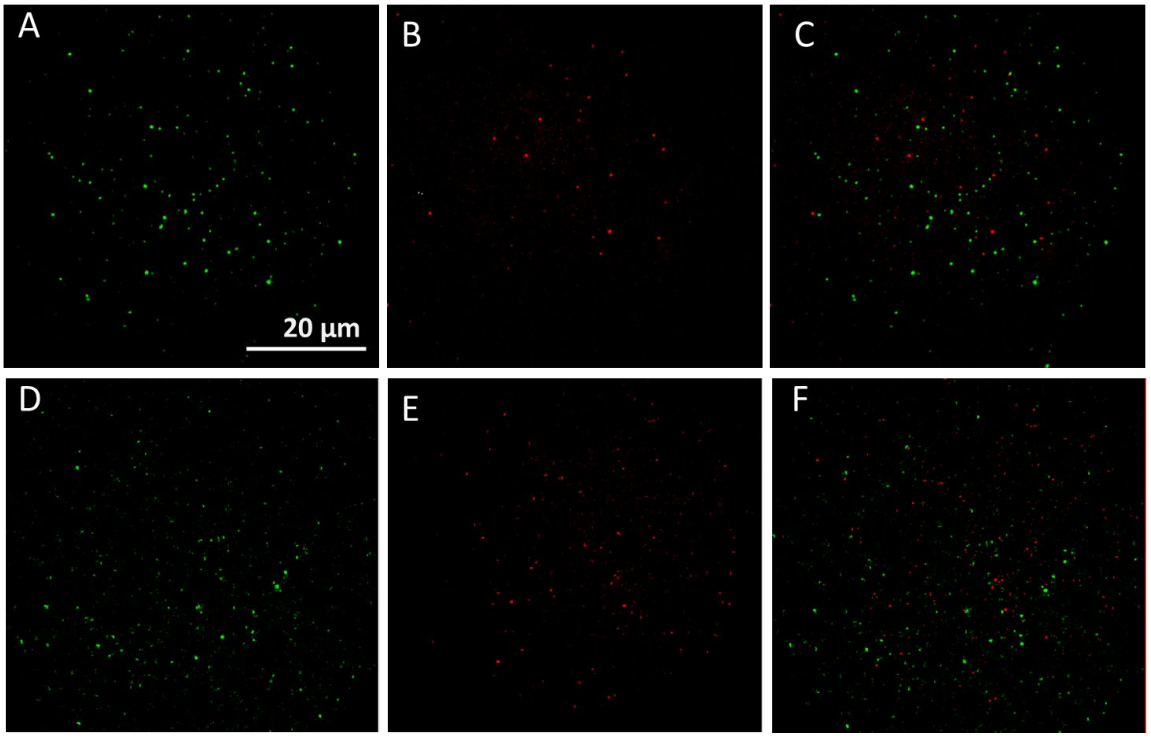

Figure 1. Comparison of single CND fluorescence at multiple excitation wavelengths. **A.** Wide field fluorescence image of non-doped CNDs (3.0 nm average size) with 561 nm excitation. **B.** The same field of view using 640 nm excitation. **C.** An overlay of A and B. **D.** Wide field fluorescence image of N-doped CNDs (3.4 nm average size) with 561 nm excitation. **E.** The same field of view as D using 640 nm excitation. **F.** An overlay of D and E. Both doped and non-doped particles show that NIR and red fluorescence originates from different particles.

particles for all diameters. We generated histograms composed of single particle intensities and used the peak of the histogram as the average intensity for each variety of CND (Supporting Information). A comparison of the average emission intensity of single CNDs for each variety of CND under epifluorescence excitation and EMCCD based detection is shown in Figure 2. For comparison intensities are normalized to the lowest value. It has previously been observed that

the absorption spectra of CNDs are the same regardless of the size from 3 nm to 12 nm[20,26]. Our results show that for non-doped CNDs the intensity of the smaller particles (~3 nm) is approximately 1.8 times higher than particles with largest size (~11 nm) at 561 nm excitation (Figure 2A). These same particles show a similar trend, though less pronounced, at 640 nm excitation- small particles are approximately 1.2 times brighter than the larger particles (Figure 2B). N-CNDs showed no significant change in average intensity for different size particles with 561 nm excitation. There was, however, a small increase (~10%) in average intensity for 12 nm doped particles compared to 3.4 nm particles at 640 nm excitation (Figure 2B). In all cases non-doped particles with 561 nm excitation exhibited higher average intensity than similar sized N-doped particles. This was most pronounced at smaller

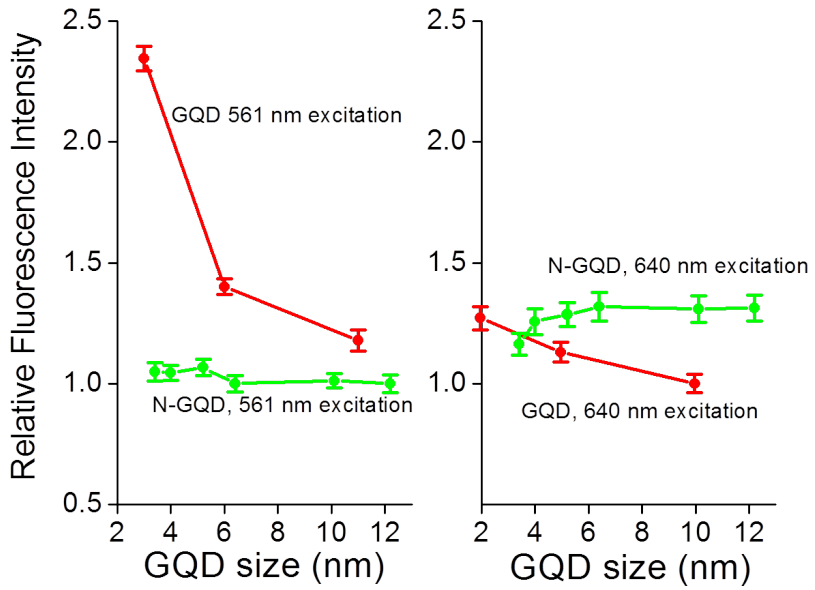

Figure 2. Fluorescence intensity variation with particle size. A. The average fluorescence intensity of non-doped (red line) and N-doped (green line) CNDs with 561 nm excitation (78W/cm²). B. The average fluorescence intensity of non-doped (red line) and N-doped (green line) CNDs with 640 nm excitation under wide field (80 W/cm²) excitation. In each graph the values are normalized to the lowest value.

sizes. At 640 nm excitation, doped and non-doped particles (CNDs) with similar size showed similar levels of fluorescence intensity with N-doped particles typically showing higher levels fluorescence (Figure 2B). The largest N-doped particle was 30% brighter on average than non-doped particles of similar size.

We also performed experiments to determine the relative population of red (561 nm excitation) particles compared to the NIR (640 nm excitation) particles for each species. Within an EMCCD field of view of isolated particles we counted the number of each species. In all non-doped samples, there was always fewer NIR (660 nm to 1000 nm) emitting particles than red (607 ±27 nm) emitting particles. The ratio of NIR to red emitting particles decreases from ~0.45 to 0.14 when the average size of the particles increases from 3 nm to 11 nm (Figure 3A). The distribution of particle populations in the N-doped CNDs is more striking. The ratio of the number of NIR to red emitting particles decreases from 1.2 to 0.17 when the average size increases from 3.4 to 5.2 nm. All the doped particles larger than 5.2 nm showed a similar ratio of ~0.17. Interestingly, this ratio is very close to the value (~0.14) observed for non-doped CNDs with average size 6 to 11 nm (Figure 3A, Supporting Information, Figure 1S). The NIR emitting species only becomes the most abundant for small doped particles. These results suggested that the observed photophysical properties could be related to the level of doping for each particle species. Subsequent tests to determine the percent dopant using electron energy loss spectroscopy (EELS) showed that the percent doping measured as N/C atomic ratio increased from 7% to 5% as the particle size decreased (Supporting Information, Figure 2S & 4S). This suggests that the observed changes in relative number of NIR emitting particles might be related to the dopant percent rather than the size. The significant effect of nitrogen dopant percentage on NIR emitting particles are consistent with previous ensemble measurements, reporting that

higher nitrogen content shifts CND emission to the red.

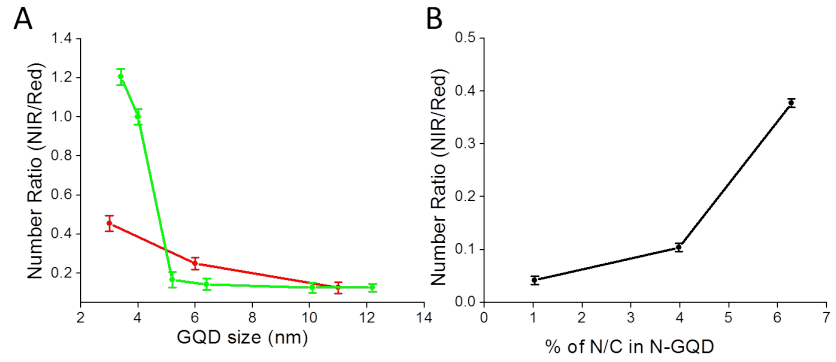

Figure 3. Variation of the ratio of the number of NIR to red emitting particles. **A.** The variation of the ratio of NIR emitting particles (640 nm excitation) to red emitting particles (561 nm excitation) for non-doped and N-doped CNDs with particle size. The red line represents non-doped CNDs and the green line N-doped CNDs. **B.** The variation of the ratio of NIR to red emitting CNDs with the N/C content of N-CNDs (average size of 6 nm).

To determine if the observed trends in the NIR emitting particles correlate to the amount of dopant in the N-CNDs, we prepared three N-CNDs with the same diameter (6 nm) but with varying amounts of nitrogen dopant. These CNDs had a N/C ratio as measured by electron energy loss spectroscopy (EELS) of 1.03%, 3.98%, and 6.28%. Single particle fluorescence imaging of these particles shows that the relative population of NIR (640 nm excitation) emitting particles compared to red (561 nm excitation) emitting particles increases with an increase of the dopant content (Figure 3B). The value increases from 0.04 to 0.38 as the N/C ratio increases from 1.03% to 6.28%. Thus, the increase in nitrogen content of particles with the same diameter resulted in an increase in the ratio of NIR emitting particles to red emitting particles. This suggests that the higher proportion of NIR emitting particles observed in smaller CNDs (~3 nm) compared to the larger ones (~12 nm) is, at least partially, a consequence of doping levels. This suggests the apparent size dependence observed in figure 3 is related to the

level of dopant. In this context, it is important to take into account that the smaller particles have a higher surface area per unit volume of CND compared to larger particles and the doping of nanoparticles is primarily a function of the surface area. Thus, the N atom content with respect to carbon content would be highest in the smaller particles. This suggests that doping is size dependent, and that dopant levels play a prominent role in NIR emission. It should be noted that we are measuring only those particles with sufficient intensities to be visible at the single particle level. It is possible that there are particles with insufficient intensity to be counted. Thus, the changes we observe could be either from changes in the distribution of the fluorophores or from changes in the intensity of the fluorescence from a particular emissive species.

We observed two trends related to the proportion of NIR emitting to red emitting particles. For non-doped samples, smaller particles (3 nm) have a moderately higher fraction of NIR particles (0.45) compared to the fraction of NIR particles (0.3) for larger particles (> 6 nm) (Figure 3A, Supporting Information Figure 1S). This suggests that NIR emission is at least partially size dependent. However, we observe the largest fraction of NIR emitting particles for 3.4-5.2 nm nitrogen doped CNDs. The smallest doped particles have a ratio of 1.2 NIR to red. This substantial increase in the fraction of NIR particles strongly suggests a correlation with the percent doping and is supported by the observation of N-CNDs with different N/C ratios (Figure 3B). This is consistent with the fact that nitrogen doping greatly narrow the bandgap of CNDs. As the size of a particle increases, the amount of doped nitrogen atoms relative to carbon content in CNDs decreases as the doping reaction rate increases with increased surface area of the nanoparticle. Thus, the percent N/C content is largest for 3.4 nm N-CNDs. It is possible that the accumulation or internalization of other elements (N, S, O etc) may result in unintended doping

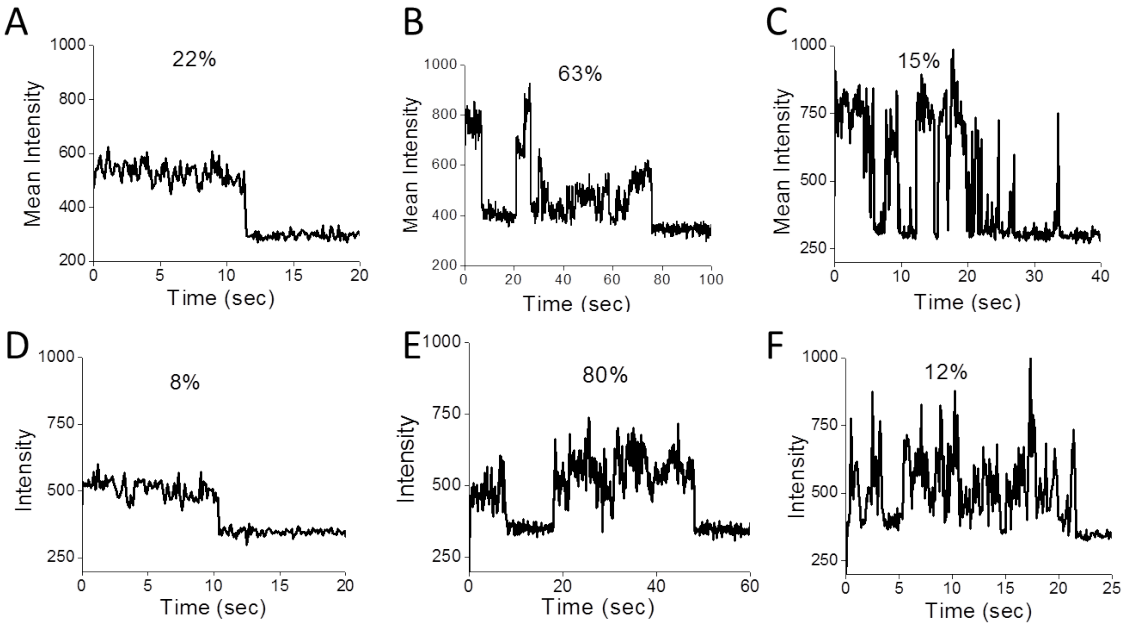

Figure 4. Single particle intensity versus time trajectories. The top row shows representative examples of single non-doped CNDs exhibiting **(A)** single level fluorescence, **(B)** multilevel fluorescence, and **(C)** blinking each extracted from wide-field imaging (100 ms exposure) with 561 nm excitation (78 W/cm²). The bottom row shows representative examples of single nitrogen-doped CNDs exhibiting **(D)** single level fluorescence, **(E)** multilevel fluorescence, and **(F)** blinking each extracted from wide-field imaging (100 ms exposure) with 561 nm excitation (78 W/cm²).

of non-doped CNDs. This unintended doping would likely be highest in the smaller particles. This could be the origin of slight increase in fraction of NIR emitting particles seen for non-doped particles. The accumulation of these other elements could occur during CND preparation from elements in the atmosphere. While the number of internalized non carbon elements would likely be very low in these CNDs, the proportion of these atoms relative to carbon increases with decreased size.

We also observed fluorescence intensity fluctuation in single CNDs during laser excitation. We categorized time traces for single particles into three groups: particles with constant

fluorescence intensity, multistep intensity fluctuations, and single step transitions between a fluorescent and a dark state (blinking). Representative single molecule time traces of non-doped (A-C) and doped (D-E) with 561 nm excitation are shown in Figure 4. Particles with constant fluorescence intensity were characterized by an initial steady fluorescence level before permanent photobleaching to the background level in a single step. The presence of multiple fluorescence intensity levels was defined by the analysis of intensity distribution histograms and the presence of multiple levels of sustained duration at a particular fluorescence intensity and not transient single frame fluctuations. Blinking particles were defined as those which exhibited fluorescence intensity fluctuations between a single emissive level to the background level and back again for multiple cycles. Table 1 shows the proportion of single particles in each of these categories. As the average size of the CNDs increase from 3 nm to 11 nm, the percent of particles exhibiting a constant fluorescence intensity and those showing blinking behavior increased from 22% to 31% and 15% to 31%, respectively. On the other hand the percent of CNDs with multi-step fluorescence fluctuation decreases from 63% to 38 % as the average size CNDs increases from 3 nm to 11 nm. This suggests a size dependence for the

Table 1. Comparison of CND intensity fluctuations (561 nm exc).

	One Step Bleaching	Multi-step Fluctuation	Blinking	# of particles
3 nm CND	22%	63%	15%	73
6 nm CND	25%	48%	27%	70
11 nm CND	31%	38%	31%	65

Table 2. Comparison of CND intensity fluctuations (640 nm exc).

	One Step Bleaching	Multi-step Fluctuation	Blinking	# of particles
3.4 nm N-CND	61%	37%	2%	72
4.0 nm N-CND	65%	30%	5%	56
5.2 nm N-CND	33%	65%	2%	48
6.4 nm N-CND	23%	72%	5%	55
12.2 nm N-CND	20%	75%	5%	40

blinking properties of non-doped CNDs with 561 nm excitation. Nitrogen doped particles exhibited no clear size dependent trends with 561 nm excitation (Supporting Information, Table 1S). Similar experiments were performed using 640 nm excitation. Representative time traces with 640 nm excitation are shown in Supporting Information, Figure 5S. These experiments yielded no observable size-dependent trends in particle characterization for non-doped CND particles (Supporting Information, Table 2S). Very few of these non-doped particles, at any size, showed blinking behavior on the time scale of our observations using 640 nm excitation. However, nitrogen doped particles did show clear trends with 640 nm excitation. The percentage of particles with a single intensity level decreased from 60% for 3.4 nm particles to ~20% for 12.2 nm. At the same time, the percentage of particles exhibiting multi-level fluorescence increased from 37% to 75% (Table 2). Thus, non-doped CNDs exhibited a trend at 561 nm excitation but not at 640 nm excitation. Nitrogen doped CNDs exhibited the opposite behavior with a clear size-dependent trend with 640 nm excitation but no apparent trend with 561 nm excitation.

We also measured the photostability of single CNDs. With 561 nm excitation (~78 kW/cm^2) the photobleaching time of all non-doped and N-doped CNDs of all sizes is between 16 sec to 22 sec (Figure 5A). There were no size dependent properties observed for CND photobleaching times with 561 nm excitation. Additionally, there was no trend in the photostability for particles of the same size but with varying nitrogen content (Figure 5C). However, both size and dopant dependent photobleaching properties were observed for 640 nm excitation. As the size increased from 3 nm to 11 nm the bleaching time decreased from 30 sec to 15 sec for non-doped CNDs. Similarly, smaller N-doped CND particles were also more photostable than larger particles with 640 nm excitation. The average photobleaching time was 95 s for 3.4 nm N-CNDs and 20 s for

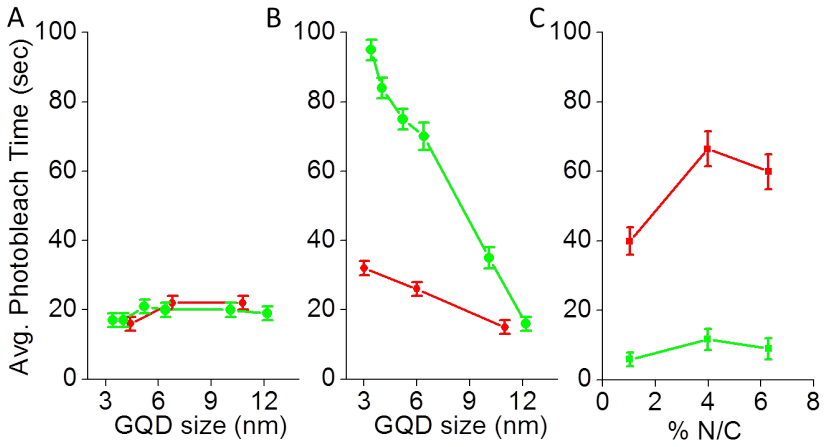

Figure 5. Variation of photobleaching times. **A.** Comparison of the average photobleaching time for each CND size with 561 nm excitation for non-doped (red line) and N-doped (green line) CNDs. **B.** Comparison of the average photobleaching time for each CND size with 640 nm excitation for non-doped (red line) and N-doped (green line) CNDs. **C.** Plot of the average photobleaching time for 6 nm particles with varying % N/C content with 561 nm excitation (green line) and 640 nm (red line).

12.2 nm (Figure 5B). Similar to the studies of NIR proportion, an increase in photostability at 640 nm excitation appears to be primarily correlated to the level of nitrogen dopant. This was verified by performing similar experiments with N-CNDs that had varying levels of dopant. The observed photobleaching time of the N-CNDs with variable amount of doped nitrogen showed a clear trend that scaled with percent dopant (Figure 5C). For particles of the same size, at 1.03% N/C particles exhibited a photobleaching time of 40 sec. This increased to 67 seconds 3.98% but did not increase further at 6.28% N/C.

In conclusion we have explored the single particle emission of N doped and non-doped CNDs with average particle sizes varying from ~3 nm to ~12 nm as well as with varying N/C content. All the samples are composites of fluorescently distinguishable particles emitting at separate

wavelengths with 488 nm, 561 nm, or 640 nm excitation. We observed moderate size dependent properties, but the percent doping played a larger role in CND photophysical properties. In particular, the properties of the NIR emitting species of nitrogen doped particles were highly dependent on the percent of dopant. Single particle studies along with steady state fluorescence studies of multiple sizes of undoped and N-doped CNDs suggests that either single particles are not capable of multiple emission bands or that the multiple emissive species observed in bulk samples come from the same particle but only one emission band is sufficiently bright enough to be observed at the single particle level. The latter possibility is consistent with our observation that 488 nm excitation yields fluorescence in bulk but these particles cannot be observed at the single particle level because they are not bright enough to be detected. These studies indicate that extent of CND doping is likely responsible for differences in NIR and red emitting single particles. Incorporation of N sites into the structure likely increases the inhomogeneity of the nanoparticle surface. It has been proposed that CND emission is in part the result of surface energy traps that serve as emissive states. Altering the surface states has also been shown to affect emissive properties leading to a red shift in emission[34,35]. Increasing the dopant level in CNDs likely modifies surface states, in our case by increasing the N content, and potentially increases the number of these surface traps. As the surface states are modified by the dopant the fluorescence is dominated by emission from these modified surface states resulting in differences in the photophysical properties of CNDs seen with varying levels of dopant.

Supporting Information. Supplemental figures. This material is available free of charge via the Internet at http://pubs.acs.org.

Present Addresses

† Nanopore Diagnostics, LLC. 2033 West port Center Dr, St. Louis, MO 63146.

Author Contributions

SKD, DYK, SPL, and CIR designed experiments and wrote the manuscript. SKD, CML, WEM, and LT performed experiments. All authors have given approval to the final version of the manuscript.

REFERENCES

(1) Liang, H.; Zhang, X. B.; Lv, Y. F.; Gong, L.; Wang, R. W. *Accounts Chem Res* **2014**, *47*, 1891.

(2) Baker, S. N.; Baker, G. A. *Angew Chem Int Edit* **2010**, *49*, 6726.

(3) Li, L. L.; Wu, G. H.; Yang, G. H.; Peng, J.; Zhao, J. W. *Nanoscale* **2013**, *5*, 4015.

(4) Abdullah-Al-Nahain; Lee, J. E.; In, I.; Lee, H.; Lee, K. D. *Mol Pharmaceut* **2013**, *10*, 3736.

(5) Wang, H. B.; Maiyalagan, T.; Wang, X. *Acs Catal* **2012**, *2*, 781.

(6) Chung, C.; Kim, Y. K.; Shin, D.; Ryoo, S. R.; Hong, B. H. *Accounts Chem Res* **2013**, *46*, 2211.

(7) Das, S. K.; Liu, Y. Y.; Yeom, S.; Kim, D. Y.; Richards, C. I. *Nano Lett* **2014**, *14*, 620.

(8) Tang, L.; Ji, R.; Li, X.; Bai, G.; Liu, C. P. *ACS Nano* **2014**, *8*, 6312.

(9) Tang, L. B.; Ji, R. B.; Cao, X. K.; Lin, J. Y.; Jiang, H. X. *ACS Nano* **2012**, *6*, 5102.

(10) Sun, Y. P.; Zhou, B.; Lin, Y.; Wang, W.; Fernando, K. A. S. *J Am Chem Soc* **2006**, *128*, 7756.

(11) Gokus, T.; Nair, R. R.; Bonetti, A.; Bohmler, M.; Lombardo, A. *ACS Nano* **2009**, *3*, 3963.

(12) Peng, H.; Travas-Sejdic, J. *Chem Mater* **2009**, *21*, 5563.

(13) Peng, J.; Gao, W.; Gupta, B. K.; Liu, Z.; Romero-Aburto, R. *Nano Lett* **2012**, *12*, 844.

(14) Zhang, J.; Li, J. J.; Wang, Z. L.; Wang, X. N.; Feng, W. *Chem Mater* **2014**, *26*, 2460.

(15) Tang, L. B.; Ji, R. B.; Li, X. M.; Bai, G. X.; Liu, C. P. *ACS Nano* **2014**, *8*, 6312.

(16) Li, H. T.; He, X. D.; Kang, Z. H.; Huang, H.; Liu, Y. *Angew Chem Int Edit* **2010**, *49*, 4430.

(17) Pan, D. Y.; Zhang, J. C.; Li, Z.; Wu, C.; Yan, X. M. *Chem Commun* **2010**, *46*, 3681.

(18) Lu, J.; Yang, J. X.; Wang, J.; Lim, A.; Wang, S. *ACS Nano* **2009**, *3*, 2367.

(19) Zhao, H. X.; Liu, L. Q.; Liu, Z. D.; Wang, Y.; Zhaoa, X. J. *Chem Commun* **2011**, *47*, 2604.

(20) Li, H. T.; Kang, Z. H.; Liu, Y.; Lee, S. T. *J Mater Chem* **2012**, *22*, 24230.

(21) Paul, R. K.; Badhulika, S.; Niyogi, S.; Haddon, R. C.; Boddu, V. M. *Carbon* **2011**, *49*, 3789.

(22) Qiao, Z. A.; Wang, Y. F.; Gao, Y.; Li, H. W.; Dai, T. Y. *Chem Commun* **2010**, *46*, 8812.

(23) Tang, L. B.; Ji, R. B.; Li, X. M.; Teng, K. S.; Lau, S. P. *Part Part Syst Char* **2013**, *30*, 523.

(24) Luk, C. M.; Chen, B. L.; Teng, K. S.; Tang, L. B.; Lau, S. P. *J Mater Chem C* **2014**, *2*, 4526.

(25) Zhang, Z. Z.; Chang, K. *Phys Rev B* **2008**, *77*.

(26) Kim, S.; Hwang, S. W.; Kim, M. K.; Shin, D. Y.; Shin, D. H. *ACS Nano* **2012**, *6*, 8203.

(27) Dong, Y.; Pang, H.; Yang, H. B.; Guo, C.; Shao, J. *Angew Chem Int Ed Engl*, *52*, 7800.

(28) Dekaliuk, M. O.; Viagin, O.; Malyukin, Y. V.; Demchenko, A. P. *Phys Chem Chem Phys*, *16*, 16075.

(29) Tang, L.; Ji, R.; Li, X.; Bai, G.; Liu, C. P. *ACS Nano* **2014**, *8*, 6312.

(30) Qu, D.; Zheng, M.; Du, P.; Zhou, Y.; Zhang, L. G. *Nanoscale* **2013**, *5*, 12272.

(31) Li, S.; Li, Y.; Cao, J.; Zhu, J.; Fan, L. *Anal Chem* **2014**, *86*, 10201.

(32) Li, X.; Lau, S. P.; Tang, L.; Ji, R.; Yang, P. *Nanoscale* **2014**, *6*, 5323.

(33) Lee, J.; Kim, K.; Park, W. I.; Kim, B. H.; Park, J. H. *Nano Letters* **2012**, *12*, 6078.

(34) Sun, Y.-P.; Zhou, B.; Lin, Y.; Wang, W.; Fernando, K. A. S. *Journal of the American Chemical Society* **2006**, *128*, 7756.

(35) Dong, Y.; Pang, H.; Yang, H. B.; Guo, C.; Shao, J. *Angewandte Chemie International Edition* **2013**, *52*, 7800.

TOC Graphic